

FATIGUE DAMAGE ASSESMENT USING THERMOELASTIC STRESS ANALYSIS

F.A. Díaz, E.A. Patterson and J.R. Yates
The University of Sheffield, Department of Mechanical Engineering,
Mappin street, Sheffield S10 3JD, U.K.
E-mail: f.a.diaz@sheffield.ac.uk
e.a.patterson@sheffield.ac.uk
j.yates@sheffield.ac.uk

Abstract

Accurate crack detection and assessment of the fatigue damage in industrial components has been a major area of interest and research over the last decades. In this sense, the ability to make reliable stress measurements at the crack tip is an essential part in the understanding of the fatigue process.

In the current work Thermoelastic Stress Analysis (TSA) is presented as a novel methodology for measuring the effective stress intensity factor from the analysis of thermoelastic images. In addition, ΔK values inferred using TSA have been employed to estimate an equivalent opening/closing load. Results have been compared with those obtained using the strain-offset technique showing an excellent level of agreement.

Introduction

In recent years, the advances in infrared thermography together with the development of infrared staring array radiometer detectors have made it possible to apply all this technology to fatigue damage assessments. Such an example is Thermoelastic Stress Analysis (TSA). This experimental technique makes it possible to infer the in-plane stresses on a solid structure by computing the small temperature changes induced as a result of a cyclic load.

From the fatigue point of view, TSA constitutes a breakthrough over other experimental stress analysis techniques. With TSA the stress intensity factor is directly obtained by computing the cyclic stress field ahead of the crack tip, which makes it possible to evaluate the actual crack driving force for the fatigue advance [1 and 2]. The outcome is that the TSA method provides a direct measurement of the effective ΔK that is usually measured indirectly by a compliance technique.

In the current work a novel approach for the calculation of ΔK from the analysis of thermoelastic images is employed to study the fatigue crack closure phenomenon. To support the idea that TSA can provide accurate information about the real fatigue crack driving force experiments have been conducted using aluminium 2024 CT specimens (Fig. 1). As a result, ΔK results obtained using thermoelastic images have been employed to infer an equivalent value for the opening/closing load for increasing R-ratios. Results have been compared with those obtained using the strain offset technique, showing in all the cases a very good level of agreement and highlighting the real potential of TSA for fatigue damage assessment.

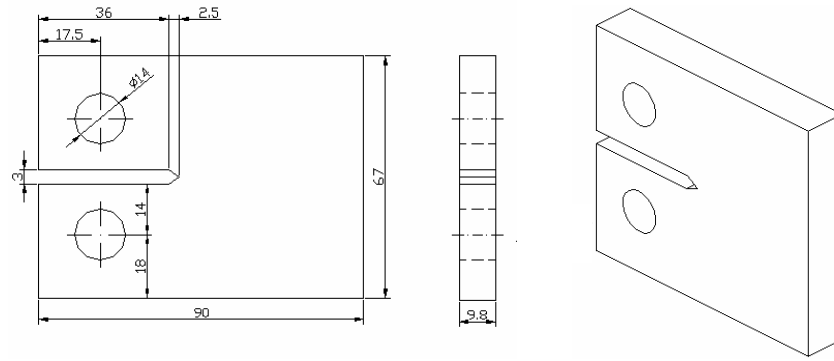


FIGURE 1. Illustration of aluminium CT specimens.

Fundamentals of TSA

TSA is a non-contacting, non-destructive and non-invasive experimental technique that provides full-field stress maps on the surface of a mechanical component based on the temperature changes that occur with applied load as result of the thermoelastic effect (Fig. 2.A). The technique measures load-correlated temperature signals in a cyclically loaded body using infrared detectors. The analysis of thermoelastic response has to be done under dynamic conditions at an adequate frequency to ensure adiabatic conditions in order to prevent heat transfer through the test piece. When adiabatic conditions are achieved and maintained during the test, the relation between the induced temperature change and the change in the sum of principal stresses is assumed to be linear, and thus the variation in the sum of principal stresses can be experimentally inferred by processing the thermoelastic signal, S .

$$\Delta(\sigma_1 + \sigma_2) = A S \quad (1)$$

Calibration of the thermoelastic signal

Thermoelastic images are normally presented referred to a scale expressed in thermal units. However, to translate the thermal units into stresses the calibration constant, A , in equation 1 must be calculated. This process consists essentially in defining the stress at a point in the images for a given load on the structure. The method adopted for calculating the calibration constant, A , consists of generating an independent measure of stress using strain gauges. For this purpose, a rosette of two orthogonal gauges is bonded to the specimen in a region of uniform stress, where the thermoelastic signal is constant.

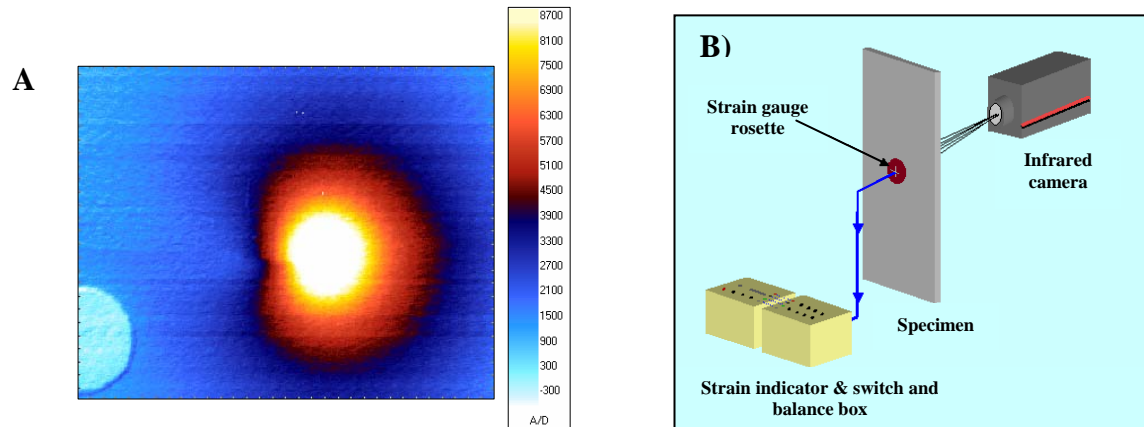


FIGURE 2. A) Typical thermoelastic pattern of a fatigue crack. B) Schematic illustration of the calibration process.

From the rosette strain gauge the first strain invariant can be obtained, and subsequently Hooke's law can be applied to derive the stresses according to the following expression:

$$\Delta(\sigma_1 + \sigma_2) = \Delta(\sigma_x + \sigma_y) = \frac{E}{1-\nu} \Delta(\varepsilon_x + \varepsilon_y) = A S \rightarrow A = \frac{\frac{E}{1-\nu} \Delta(\varepsilon_x + \varepsilon_y)}{S} \quad (2)$$

Where, E , is the Young's modulus, ν , is the Poisson's ratio, ε_x and ε_y , are the strains in two orthogonal directions and, S , is the thermoelastic signal.

Finally, by correlating the thermoelastic signal corresponding to the location of the rosette strain gauge with the sum of the principal stresses derived from the strain gauge, the calibration constant can be calculated. A schematic illustration of the calibration process is presented in Fig. 2.B.

Operational features of the thermoelastic equipment

The equipment employed for this analysis is the latest version of Deltatherm system, DT 1500, produced by Stress Photonics Inc. This system incorporates a focal plane staring array detector, which makes it possible to simultaneously collect thermoelastic data from a window of 320 by 256 pixels at an adjustable frame rate up to 158 frames per second (Fig. 3.A), reducing considerably the time for data collection. Each discrete value at a specific point on the test object surface is then sensed by one of the many thousands of single Indium Antimonide detectors (In-Sb). This particular type of detector when cooled to 77° K has an operational wavelength in the range of 2 to 5 μm . For the case of DT 1500, the focal plane array is refrigerated using a closed circuit cooling system. The system also has a maximum thermal resolution of 2 mK full field with a maximum 25 μm spatial resolution when using the maximum optical magnification.

Sample preparation for thermoelastic testing

The specimen morphology selected for the experiments reported in the current work were CT specimens made of aluminium 2024, as illustrated in Fig. 1. Specimens were initially treated to increase their surface emissivity and enhance their thermoelastic pattern by spraying them with a black matt paint (type RS 496-782).

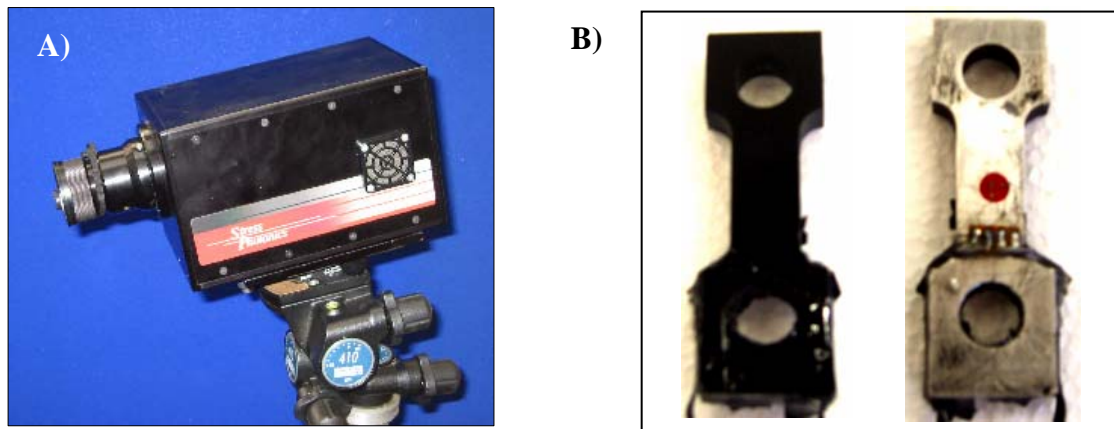


FIGURE 3. A) DT 1500 system. B) Detail of the tensile bar employed for the calculation preparation of the thermoelastic calibration constant, A.

For the calculation of the thermoelastic calibration constant, A , a tensile plate made with the same material was employed. As for CT specimens the front side of the tensile plate was also painted black. In addition, a rosette strain gauge (Tokyo Sokki Kenkyujo Co., Ltd., type FPA-2-11, 2 mm, $120 \pm 0.5 \Omega$) was also bonded at the centre of the rear face of the tensile specimen (Fig. 3.B).

Calculation of the SIF range from thermoelastic images

Different approaches have been developed in recent years as general methods for calculating the SIF from the analysis of thermoelastic images. Some of these approaches act by fitting a mathematical model describing the near crack tip stress field to a set of experimental data points collected at the near crack tip region [3 and 4]. As a result of the mathematical fitting the SIF can be inferred. The adopted method for calculating the SIF is based on a Multi-Point Over-Deterministic (MPOD) method [5] in conjunction with a description of the near crack tip stress field based on Muskhelishvili's complex potentials [6].

The algorithm developed by the authors [1 and 2] for calculating the SIF employs a combination of two iterative numerical methods, namely a genetic algorithm (GA) and the Downhill simplex method. In addition, the algorithm also includes a local search routine to locate the crack tip location from the processing of the thermoelastic image. This constitutes a major improvement over previous methods where the crack tip position is obtained by direct observations of the thermoelastic pattern. Direct observation of the crack tip is often difficult since data very near the crack tip tends to be blurred as a result of plasticity and the presence of high stress gradients.

To calculate ΔK using TSA, it is required to obtain a thermoelastic map of the region near the crack tip. Subsequently, a set of data points has to be collected in the region surrounding the crack tip. In this sense care must be taken to avoid collecting data points at those locations affected by near crack tip plasticity. Subsequently, the coordinates of the selected data points and the value of their thermoelastic signal are supplied as an input to a computer program which performs the image analysis. Finally, the mode I and the mode II SIF ranges and the crack tip coordinates are inferred. In all cases the quality of the mathematical fitting is assessed by the mean and the variance of the fit. The method is schematically described in (Fig. 4).

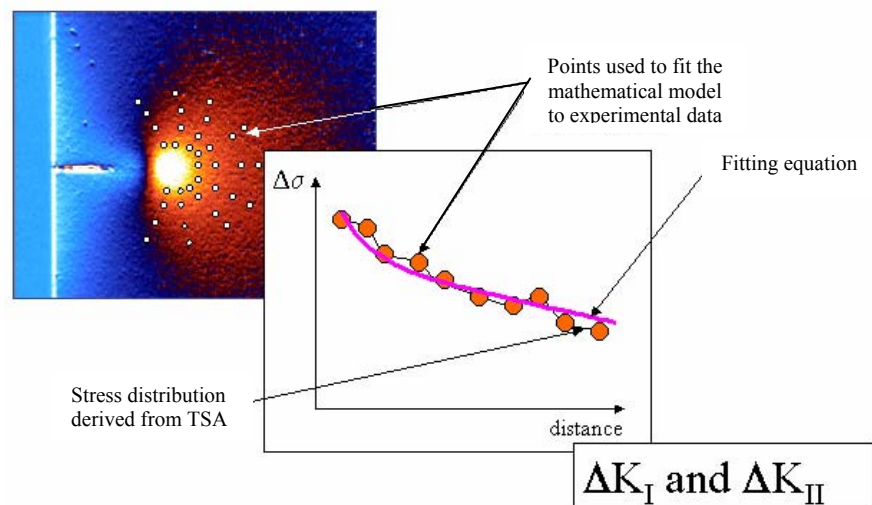


FIGURE 4. Schematic illustration of the methodology for calculating the stress intensity factor from thermoelastic data.

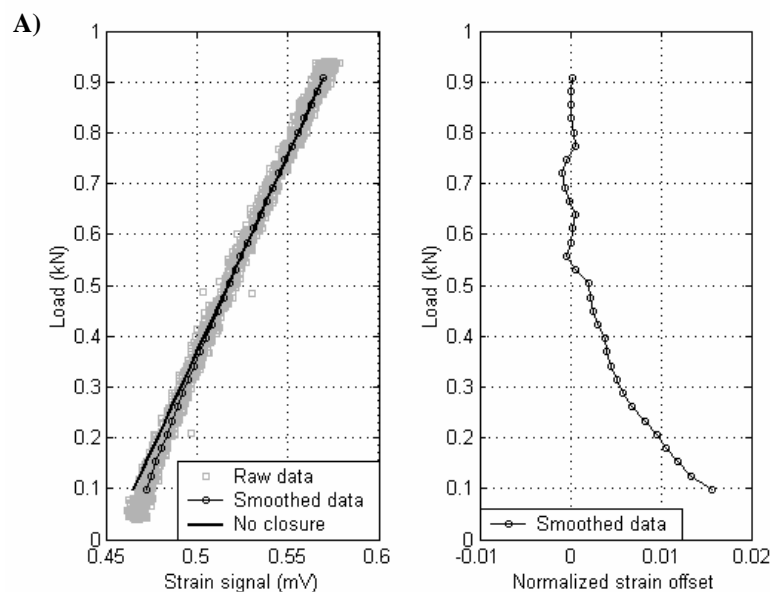
Calculation of the opening load from the analysis of the compliance traces

To detect the change in compliance as a crack closes prematurely, specimens were prepared by bonding strain gauges (Tokyo Sokki Kenkyujo Co., Ltd., type FPA-2-11, 2 mm, $120 \pm 0.5 \Omega$) at three different locations. Two of the strain gauges were located near the crack tip, on the specimen surface at 62 mm from the edge of the specimen in line with the notch. One of them was aligned with the notch direction while the other was inclined at 45° with respect to the notch line (Fig. 6.A). The third strain gauge was located at the middle part of the back of the specimen (Fig. 6.A). Subsequently, cyclic loading was applied and the strain signal together with the load signal taken directly from the load cell of the hydraulic system were processed using a digital data acquisition system.

The equipment employed for this purpose consisted of a PC (Viglen-Pentium 200 MHz Intel processor) provided with an enhanced multifunction I/O PCI board (National Instruments model PCI 6052E) connected to a BNC accessory (National Instrument model BNC-2090). The system was commanded under Lab View software version 6.0 and made it possible to store load and strain data corresponding to a loading-unloading cycle as ASCII files.

Since data were affected by random noise, it was required to employ a noise reduction technique. The technique adopted was an incremental polynomial method similar to the recommended ASTM method for data reduction in fatigue tests [7]. Subsequently, for the calculation of the opening/closing loads the strain offset technique was adopted [8]. Initially, data was divided into two sets according to the loading and the unloading branches and plotted as load versus strain plots. The unloading branch was first employed to determine the specimen compliance in the absence of closure by fitting a first order polynomial to its upper part. After that, the fitted first order polynomial was employed to perform the strain-offset calculation, which consisted of subtracting the actual strain data (affected by closure) from the fitted equation (not affected by closure). Subsequently, the load against strain-offset was plotted to estimate the closing load. The closing load was then calculated as the points where data in the plot last crossed the zero strain offset (Fig. 5.A).

For the loading branch an identical methodology was followed. However, in this case the strain-offset calculation was performed using the same fitting first order polynomial obtained for the unloading branch. Finally, the opening load was calculated following the same criteria as previously adopted for the unloading branch (Fig. 5.B).



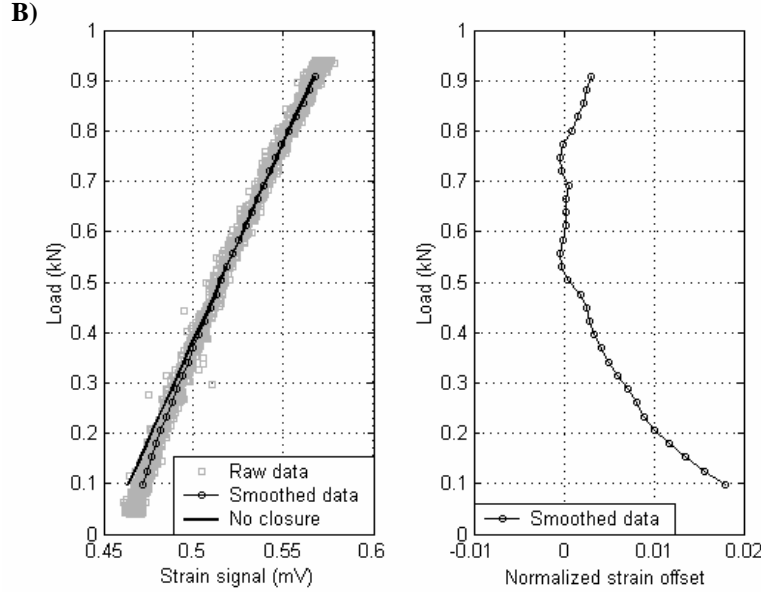


FIGURE 5. Illustration showing load vs. strain and load vs. strain-offset plots for a 42 mm crack in an aluminium CT specimen loaded between 0.94 and 0.04 kN (R-ratio 0.04). A) Unloading branch. B) Loading branch.

Experimental results

The specimen was initially pre-cracked with the crack grown until it was approximately 3 mm from the two surface strain gauges (42 mm crack length). The testing frequency was 12 Hz. Subsequently increasing load steps were gradually applied with the aim of increasing the R-ratio. For each load step, several load and strain readings were collected over a period of 0.2 s using the three strain gauges. After that, the collected data files were processed and the opening/closing loads estimated using the strain offset technique, as previously described. Results corresponding to the opening and closing loads estimated from data at the different locations (horizontal, 45° and back face) are presented in Figs. 6.B, 6.C and 6.D.

At the same time as the previous experiment, thermoelastic images were captured at each load step from the front of the specimen using DT 1500. Subsequently, thermoelastic images were processed and the stress intensity factor calculated. ΔK results from TSA were compared to the nominal ΔK [9] for the R-ratios achieved by the increasing applied load steps (Fig 7.A).

$$\Delta K_{nom} = \frac{\Delta P f(\alpha)}{t\sqrt{W}}, \quad \alpha = \frac{a}{W} \quad (3)$$

$$f(\alpha) = \frac{2 + \alpha}{(1 - \alpha)^{3/2}} (0.886 + 4.64\alpha - 13.32\alpha^2 + 14.72\alpha^3 - 5.6\alpha^4)$$

Where ΔP is the load range, a is the crack length and t and W are the specimen thickness and width respectively.

To proceed to a direct comparison of thermoelastic results with those previously obtained from the analysis of the compliance traces, ΔK values inferred from TSA were also employed to calculate an equivalent opening/closing load according to equation 3. As for the case of compliance-based techniques, the equivalent opening load was plotted for the R-ratios corresponding to every load step and compared to the maximum and minimum applied loads. Results are presented in Fig. 7.B.

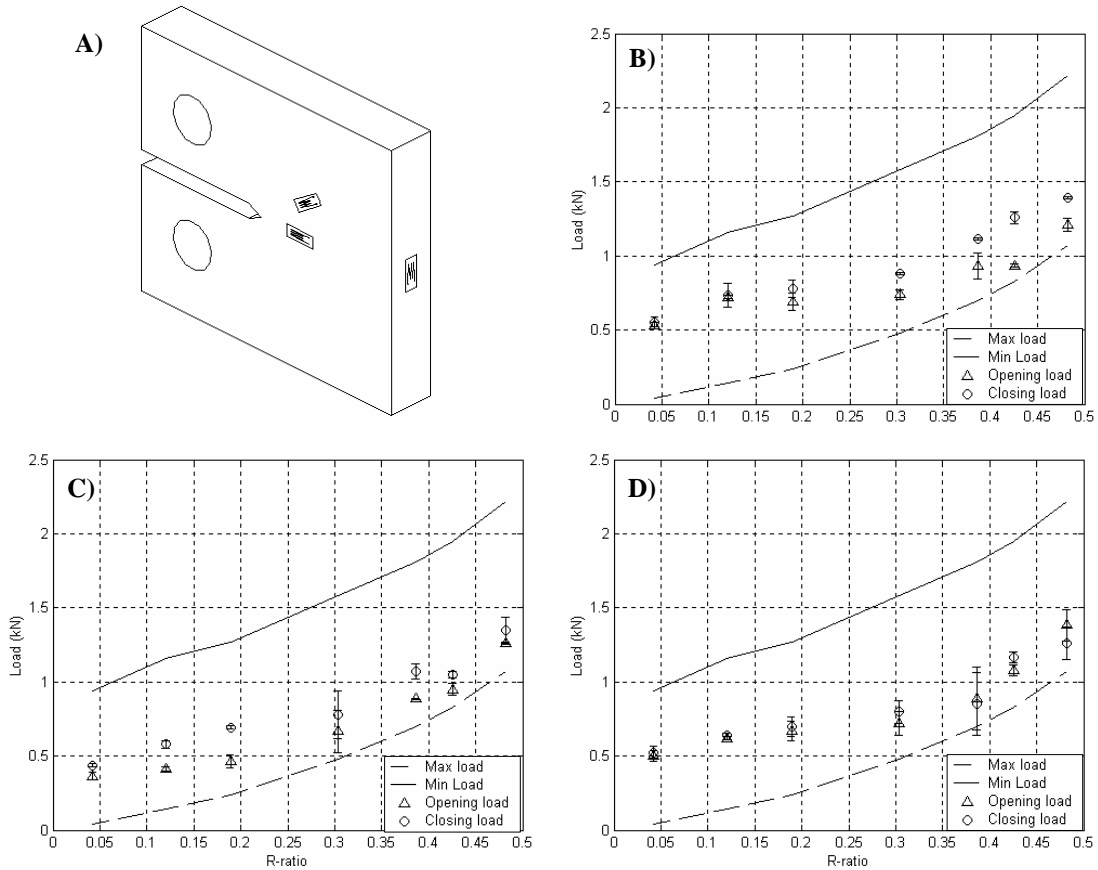


FIGURE 6. A) Scheme showing the location and orientation of the strain gauges employed for the calculation of the opening and closing loads from the compliance traces B) Illustration showing the variation of the opening and closing loads with the R-ratio for a 42 mm crack using a horizontal strain gauge, C) a 45° strain gauge, D) a back face strain gauge.

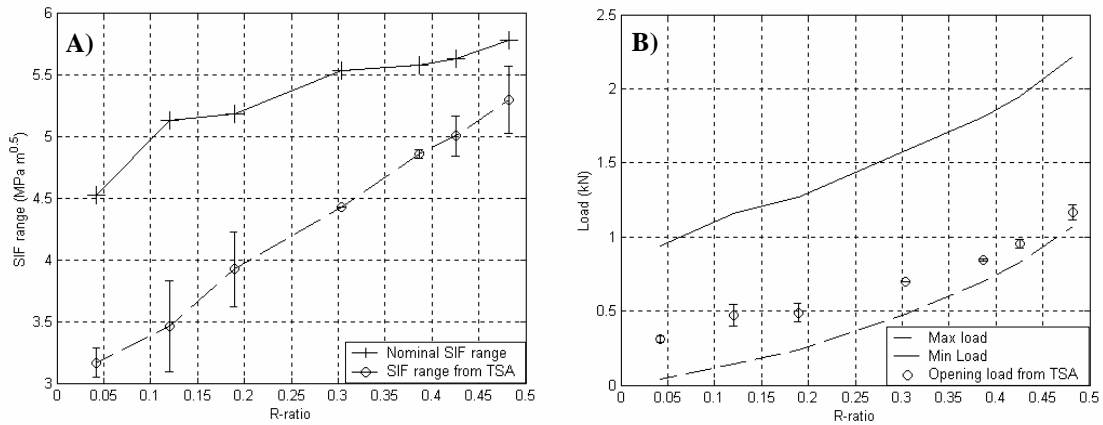


FIGURE 7. A) Plot showing the variation of ΔK with the R-ratio for a sequence of thermoelastic images corresponding to a 42 mm crack. B) Plot illustrating the variation with the R-ratio of the opening load inferred from a sequence of thermoelastic images.

Discussion

The initial aspect investigated was the repeatability of the results based on compliance measurements when using strain gauges bonded at the three locations when applying increasing R-ratio steps. Results for the opening/closing were observed in all the cases to give

similar results, with slightly smaller values for the case of the 45° strain gauge (Fig.6.B, C and D). In addition, it was also observed that as the R-ratio increased from 0.04 to 0.3, the opening/closing loads remained relatively constant and in all the cases with values higher than the minimum load. This clearly showed the presence of closure at low R-ratios. However, as the R-ratio increased from 0.3 upwards, the opening/closing load was observed to follow the minimum load indicating a considerably reduction in the closure levels.

To check the ability of TSA to successfully infer the effective ΔK , thermoelastic images were captured at the same R-ratio steps simultaneously with compliance experiments. Results for ΔK obtained from the analysis of the thermoelastic images (Fig. 7.A) show the same behaviour as observed in the compliance analysis. As the R-ratio increases the ΔK from TSA tends to approach the nominal ΔK , showing a reduction in the closure level as the R-ratio increases. Moreover, for direct comparison of thermoelastic results with those previously obtained using the strain-offset technique an equivalent opening/closing load was inferred from thermoelastic values of ΔK using equation 3 (Fig. 7.B). Results were observed to follow the same tendency as previous results obtained using the strain-offset technique for increasing R-ratio with very similar values to those obtained using the 45° strain gauge. This issue clearly support the ability of TSA to measure the effective ΔK rather than the nominal ΔK and thus the ability of the technique to measure the real crack driving force.

Conclusions

TSA has been presented as a novel technique for the study of fatigue crack closure using aluminium CT specimens. Results from TSA have been compared with those obtained using a standard technique for crack closure measurement namely, the strain-offset technique. Compliance results have clearly shown the presence of crack closure at low R-ratios in the analysed samples. Moreover, results inferred from the analysis of thermoelastic images have been observed to be in excellent agreement with those obtained using the strain offset technique, showing the ability of TSA to measure the effective ΔK .

References

1. Díaz, F.A., Yates, J.R. and Patterson, E.A., *Int. J. Fatigue*, vol. **26**, 4, 365-376, 2004.
2. Díaz, F.A., Patterson, E.A., Tomlinson R.A. and Yates, J.R., to appear in *Fat. Fract. Eng. Mat. Struct.*, vol. **27**, 2004.
3. Lesniak, J. R. and Boyce, B. R., Proceedings of SEM Spring Conference on Experimental Mechanics, Baltimore, Maryland, 491-497, 1994.
4. Tomlinson, R. A., Nurse, A. D. and Patterson, E.A., *Fat. Fract. Eng. Mat. Struct.*, vol. **20**, 217-226, 1997.
5. Sanford, R. and Dally, J. W., *Eng. Fract. Mech.*, vol. **11**, 621-633, 1979.
6. Muskhelishvili, N. I. 'Some basic problems of the mathematical theory of elasticity'. Third edition, Noordhoff Ltd., Groningen, Holland, 1953.
7. ASTM, E647-95a, American Society of Testing and Materials, vol. 03.01, 1999.
8. Skorupa, M., Beretta, S., Carboni, M. and Machniewicz, T., *Fat. Fract. Eng. Mat. Struct.*, vol. **25**, 261-273, 2002.
9. Murakami, Y., *Stress Intensity Factors Handbook*, Pergamon, Oxford, 1987.